Chapter 3
A Supersonic Crowdion in Mica

Ultradiscrete Kinks with Energy Between ^{40}K Recoil and Transmission Sputtering

Juan F.R. Archilla, Yuriy A. Kosevich, Noé Jiménez, Víctor J. Sánchez-Morcillo and Luis M. García-Raffi

Abstract In this chapter we analyze in detail the behaviour and properties of the kinks found in an one dimensional model for the close packed rows of potassium ions in mica muscovite. The model includes realistic potentials obtained from the physics of the problem, ion bombardment experiments and molecular dynamics fitted to experiments. These kinks are supersonic and have an unique velocity and energy. They are ultradiscrete involving the translation of an interstitial ion, which is the reason they are called *crowdions*. Their energy is below the most probable source of energy, the decay of the ^{40}K isotope and above the energy needed to eject an atom from the mineral, a phenomenon that has been observed experimentally.

J.F.R. Archilla (✉)
Group of Nonlinear Physics, Departamento de Física Aplicada I, Universidad de Sevilla, Avda Reina Mercedes s/n, 41012 Sevilla, Spain
e-mail: archilla@us.es

Yu.A. Kosevich
Semenov Institute of Chemical Physics, Russian Academy of Sciences, Kosygin Street 4, 119991 Moscow, Russia
e-mail: yukosevich@gmail.com

N. Jiménez · V.J. Sánchez-Morcillo
Instituto de Investigación para la Gestión Integrada de las Zonas Costeras, Universidad Politécnica de Valencia, C/.Paranimfo 1, 46730 Grao de Gandia, Spain
e-mail: nojigon@epsg.upv.es

V.J. Sánchez-Morcillo
e-mail: victorsm@upv.es

L.M. García-Raffi
Instituto Universitario de Matemática Pura y Aplicada, Universidad Politécnica de Valencia, Camino de Vera s/n, 46022 Valencia, Spain
e-mail: lmgarcia@mat.upv.es

© Springer International Publishing Switzerland 2015

J.F.R. Archilla et al. (eds.), *Quodons in Mica*, Springer Series in Materials Science 221, DOI 10.1007/978-3-319-21045-2_3

3.1 Introduction

Some materials are able to record the passage of charged particles and are used as radiation detectors [7, 9] and there are minerals that show nuclear tracks that were produced at some stage during their formation [22]. The mineral mica muscovite has been shown to have recorded the tracks of muons, positrons and other swift particles with positive charge while being deep underground [23–25]. The most recent reviews are the chapters *Tracks in mica: 50 years later* and *I saw a crystal* in this book [26, 27]. The tracks are recorded within the cation layer of potassium ions which form a two-dimensional hexagonal lattice. There are also many tracks along the close packed directions of this lattice that cannot be produced by charged particles and are attributed to some vibrational entities called *quodons* because of their quasi one-dimensional structure [28, 29, 31, 33]. Their existence has also been shown directly with an experiment in which the energy of alpha particles incident on one side of a mica specimen was able to eject atoms at the opposite border along the cation lattice directions [30].

Recently, a model with realistic potentials for the dynamics of potassium ions within the cation layer of mica muscovite has been introduced [1–3]. The authors have considered the available potentials for the interaction between atoms and ions. For the interaction between potassium ions K^+ the electrical potential was not enough because the passage of the kink brings about very short distances, for which the ions can no longer be described as point charges. Therefore, the Ziegler-Biersack-Littmark (ZBL) potential was used [36]. This potential models the electrical repulsion by the *nuclei* partially screened by the electron cloud. ZBL potentials have been widely tested and compared to data obtained in ion bombardment experiments, being therefore the more realistic ones while using classical mechanics. Quantum calculations could certainly provide more accuracy but at the cost of much more complex analytical and numerical calculations. The interaction of the potassium ions with the lattice was described with empirical potentials used in molecular dynamics and fitted with thermodynamic properties, neutron [5] and infrared spectroscopy [6] and also validated for other silicates [11].

Arguably, the most important result in the full system with substrate was that a supersonic kink was formed with specific energy and velocity [3]. As it involves the movement of an interstitial atom through the lattice, it will be called a (supersonic) *crowdion* in this chapter as described in [13]. The term will be reserved for this specific supersonic kink with stable and unique velocity and not for other kinks. If the lattice was given more energy, nonlinear waves and later phonons were emitted until the specific velocity and energy was reached. This characteristic of supersonic kinks associated with specific values of the velocity have also been described in [32, 37], where they use the terms topological soliton and lattice soliton.

The supersonic crowdion found in the mica model is extremely discrete as basically only two ions are moving at the same time, which will be referred to as the *magic mode with sinusoidal waveform* and corresponds to a phase delay very close to $q = 2\pi/3$ [14, 15] as explained below. In the *magic mode*, which was

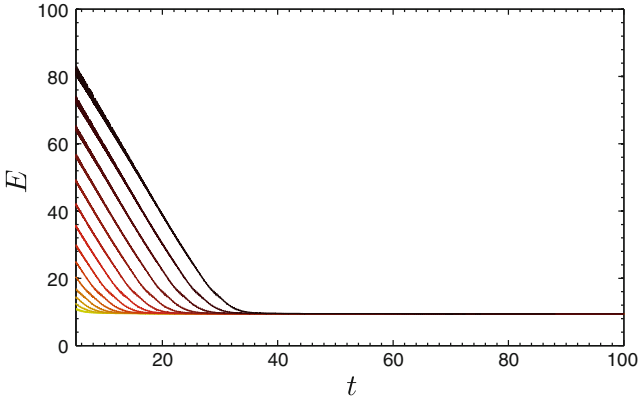


Fig. 3.1 Energies of several kinks with respect to time. When more energy than the crowdion's one is delivered and therefore a faster kink is produced, a radiation process takes place until the supersonic crowdion is formed. Thereafter, the crowdion is extremely stable. If the initial energy is smaller than the crowdion's one the kink dissipates into phonons. The scaled units are approximately 3 eV for energy and 0.2 ps for time. The final velocity and energy are approached asymptotically, being $V_c = 2.7387$ (7.2 km/s) and $E_k = 9.5$ (26.2 eV) in scaled and physical units

introduced in the Fermi-Pasta-Ulam lattice to describe both steady-state or slowly-moving breathers and supersonic kinks [14], only two particles are mostly involved in the motion at the same time. The mode with mode $q = \pi$ is the limit of discreteness as only one particle is moving at the same time, and the kink is equivalent to just one particle hitting the following one with a hard-sphere interaction. We have also called these kinks *ultradiscrete kinks* (UDK). They are also known as kinks with atomic scale localization and have been described theoretically [10] and observed experimentally in a chain of repelling magnets [19]. The energy dissipated by the crowdion and its subsequent stability can be seen in Fig. 3.1. Supersonic kinks with a discrete set of velocities for which there is no radiation have been described in previous publications [13, 18, 32, 37]. They appear in systems with substrate potential and nonlinear coupling and can be described as multiple solitons. In our system due to the extreme discreteness of the kinks there is only a non-radiating velocity corresponding to a double soliton as will be explained in Sect. 3.4. See also [3]. The structure of mica muscovite can be seen in Figs. 3.2 and 3.3 represents the coordinates of the potassium ions obtained in a numerical simulation.

The energy of the crowdion is approximately $E_k = 26.2$ eV, which is an interesting result because there are sources of energy in the lattice which can provide it as it will be explained with more detail in Sect. 3.7. The most abundant of the unstable potassium isotopes is ^{40}K, which can decay by different beta processes providing recoil energies up to 50 eV. The crowdion energy is also smaller than the second ionization energy of potassium, that is, 31.6 eV [17], which thus prevents the possibility of inelastic collisions where the kinetic energy would be lost stopping the propagation of the kink. It is also larger that the 4–8 eV needed to eject an atom [16], an effect that has been found in an experiment where the transmission of localized

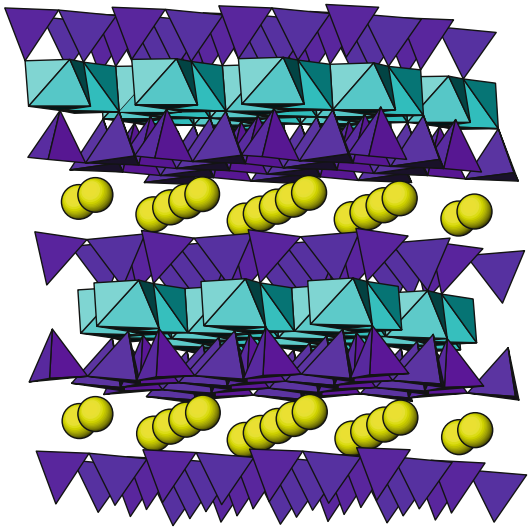


Fig. 3.2 The structure of mica muscovite where the potassium layer can be observed. This point of view has been chosen to emphasize the K^+ rows represented by *yellow balls*

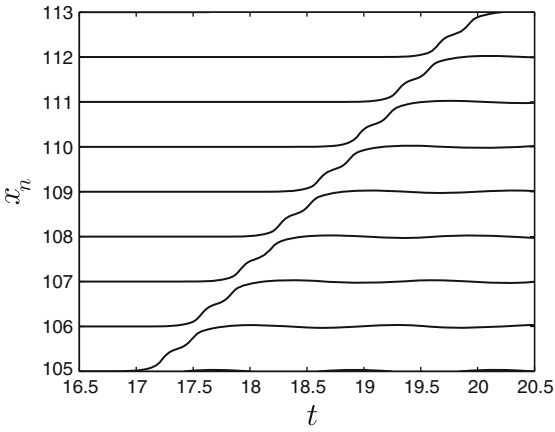


Fig. 3.3 Coordinates of the supersonic crowdion or ultradiscrete kink from numerical simulations. It can be observed that only two particles are moving at the same time. Lattice units $a = 5.19\,\text{Å}$ for coordinates and scaled units (0.2 ps) for time. Also the double kink structure can be seen as will be explained later in the text

energy along lattice directions with the subsequent ejection of an atom at the edge of the boundary has been observed [30].

Another point of interest of the crowdion is that it is equivalent to a charged interstitial K^+, i.e. an excess of an unit of elemental charge, travelling at twice the speed of sound. Therefore, it is very likely to be recorded, as positively charged particles leave tracks in mica muscovite.

Are the quodons observed in mica muscovite the crowdions described in this chapter? It is not clear, but there are several points in their favour: (a) They have an energy that can be produced by the recoil of ^{40}K; (b) They have enough energy to expel an atom at the surface; (c) They have stability and seem to travel forever; (d) They survive to room and higher temperatures; (e) They transport positive charge that would leave a track in mica muscovite. Against them is that their existence and

stability has not been verified in two or three dimensions. But even if their energy spreads they are likely to leave some of the other dark marks in mica.

The sketch of this chapter is as following: Sect. 3.2 describes the system and potentials. In Sect. 3.3 the magic mode is described with detail and the quantities in the fundamental ansatz are redefined in a new meaningful way. Section 3.4 describes the properties of the kinks when the substrate potential is introduced and the supersonic crowdion appears, while Sect. 3.5 describes the properties of phonons in a system with a substrate and applies them to analyze the crowdion's phonon tail. Some interesting results of the outcome of numerical simulations when excess energy is delivered and when the system is previously thermalized are presented in Sect. 3.6. The recoil energies in the different decay modes of ^{40}K and their consequences for the formation of kinks or other lattice excitations are described in Sect. 3.7. The chapter ends with a summary.

3.2 Description of the System

Mica muscovite is a layered silicate where a layer of potassium ions is sandwiched between layers of a complex silicate structure of tetrahedra and octahedra. This cation layer has a hexagonal structure where rows of potassium ions can be identified, as seen in Fig. 3.2. As explained with more detail in [1–3] we consider an 1D model for a row of K^+ ions. The distance between ions is $a = 5.19$ Å which in scaled units will be taken as the unit of distance. The interaction between ions is described by two terms, the first one is the electrostatic Coulomb repulsion

$$U_C = K_e \frac{e^2}{r} - K_e \frac{e^2}{a}, \tag{3.1}$$

where K_e is the Coulomb constant, e the elementary unit of charge and $r = d_n = x_n - x_{n-1}$ is the interatomic distance. The reference level of energy is taken as the electrostatic energy at the equilibrium distance a. This value of energy $K_e e^2/a = 2.7746$ eV is also taken as the unit of energy in scaled units, and it is useful to remember that it is approximately $u_E \sim 3$ eV. The other natural units are the potassium mass $m_K = 39.1$ amu and therefore the derived unit of time $\tau = \sqrt{m_K a^3/K_e e^2} = 0.1984$ ps $\simeq 0.2$ ps.

This system supports propagating kinks of almost any velocity and energy [1–3] but with very small inter-particle distances for which the ions cannot be described as point particles. The second term for short-range repulsion is the Ziegler-Biersack-Littmark or ZBL potential, which corresponds to the electrostatic interaction between nuclei partially shielded by the electron cloud which is described by an universal function that has been tested with experiments of ion bombardment [36]. The ZBL potential usually involves four terms which are effective at different ranges of energies. For the potassium atoms at energies up to 200 keV it is enough to consider a single term given by

$$U_{\mathrm{ZBL}}(r) = \frac{\alpha}{r} \exp(-\frac{r}{\rho}), \tag{3.2}$$

with $\alpha = 2650.6\,\text{eV}\,\text{Å}$ and $\rho = 0.29529\,\text{Å}$ which correspond to $\alpha = 184.1$ and $\rho = 0.0569$ in scaled units, respectively. No attractive Van der Waals term is considered as it would be much weaker than the repulsive term. The system with Coulomb and ZBL potential also support propagating kinks with many energies but with realistic distances between particles [3].

The interaction with the atoms in the lattice above and below the potassium layer is obtained from an unrelaxed lattice using empirical potentials used in molecular dynamics and fitted with thermodynamic and spectroscopic properties [5, 11] which are also valid for other silicates. The resulting periodic potential can be written as a Fourier series for which it is enough to retain the first five terms [3]

$$U_s(x) = \sum_{n=0}^{4} U_n \cos\left(2\pi\, n\, \frac{x}{a}\right). \tag{3.3}$$

The Fourier coefficients are given by

$$\begin{aligned} U_n &= [6.7902, -9.2920, 3.0512, -0.6387, 0.0891]\,\text{eV} \\ &= [2.4473, -3.3490, 1.0997, -0.2302, 0.0321], \end{aligned} \tag{3.4}$$

with the latter values given in scaled units. As will be shown later, the linear spatial frequency for the long wavelength limit becomes $119\,\text{cm}^{-1}$, that is quite close to the experimental one of $110\,\text{cm}^{-1}$ obtained with infrared spectroscopy [6]. A comparison between the three potentials can be seen in Fig. 3.4.

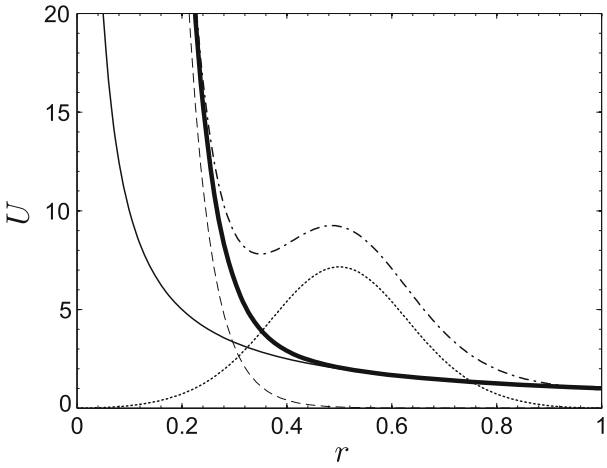


Fig. 3.4 Interaction potentials U(r) in scaled units. Coulomb (—); ZBL (− −); Coulomb+ZBL (thick −); substrate potential (· · ·) and the sum of the Coulomb, ZBL and substrate potentials (− · −). The scaled units are 2.77 eV and the lattice unit $a = 5.19\,\text{Å}$ for U and r, respectively

3.3 The Magic Mode Revisited

In this section we describe the fundamental ansatz and the variables involved. We will define the variables in a proper way, as they are not the same as in plane waves in spite of their analytic similarity. We will use scaled units for which the equilibrium interatomic distance is the unity as described above except where stated otherwise.

3.3.1 Basic Variables

Some variables used throughout the study are introduced here, together with their definitions:

Position x_n	It describes the position of the particle labelled n. At equilibrium $x_n = na$, although the origin of n is arbitrary.
Displacement u_n	It is the separation of the particle n from the equilibrium position, that is $u_n = x_n - na$.
Interatomic distance d_n	It is the distance between two particles or ions. At equilibrium it is equal to the lattice unit a, which in lattice units is the unity, but it will be written often explicitly for clarity. It is related with the positions and displacements as $d_n = x_n - x_{n-1} = u_n - u_{n-1} + a$.
Strain v_n	The increase of d_n with respect to the equilibrium distance, i.e. $v_n = d_n - a$. It is always negative for the kinks described in this chapter. It is related with the displacements as: $v_n = u_n - u_{n-1}$.
Compression c_n	The decrease of d_n with respect to the equilibrium distance, i.e. $c_n = a - d_n = -v_n$. It is always positive for the kinks described in this chapter. It is related to the displacements as: $c_n = u_{n-1} - u_n$.

3.3.2 Fundamental Ansatz

As demonstrated in [14, 15] for a large set of kink solutions of Fermi-Pasta-Ulam systems, the strain $v_n = u_n - u_{n-1}$ can be approximately described by the *fundamental ansatz with sinusoidal waveform*:

$$v_n = -\frac{A}{2}(1 + \cos(q(na - Vt))) \quad \text{with} \quad -\pi \leq q(na - Vt) < \pi, \tag{3.5}$$

where $q = 2\pi/3a$ or $q = 2\pi/3$ in scaled units with $a = 1$ that we will usually use. The value of v_n is always negative representing a compression of the bond.

This ansatz describes a moving profile with velocity V that it is better visualized in the alternative form $v_n = -A\cos^2(q/2(n - Vt))$. At any given time its value is zero except for a length $\lambda = 2\pi/q$ representing the number of consecutive bonds compressed. For a given bond n the value of v_n is zero except for an interval of time $T = 2\pi/(qV)$ representing the time during which the bond is compressed. Note that λ is not a wavelength as there is no periodic wave and T is not a period as there is no periodicity in time.

For convenience we will often use the equivalent expression for the compressions $c_n = -v_n$:

$$c_n = \frac{A}{2}(1 + \cos(\omega t - qn)) \quad \text{with} \quad -\pi \leq \omega t - qn < \pi, \tag{3.6}$$

where $\omega = qV$ is the rate of variation of the phase $\phi(n,t) = \omega t - qn$, i.e., $\omega = \partial\phi(n,t)/\partial t$ but it is not the frequency as there is no periodicity. This equation will be used in the next subsection as it is easier to interpret because c_n is always positive, the phase increases in time and the bonds compressed later have smaller phase.

From the fundamental ansatz the displacement can be constructed and it may be instructive to compare them with other solutions. They can be seen in Fig. 3.5 for the magic mode $q = 2\pi/3$ compared with the first solutions for supersonic crowdions [13]. The compressions $c_n = u_{n-1} - u_n$ have a solitonic form and in the same figure they are compared with the discretization of the solutions for the KdV equation, which describes waves in a canal [12], one of the first examples of solitons.

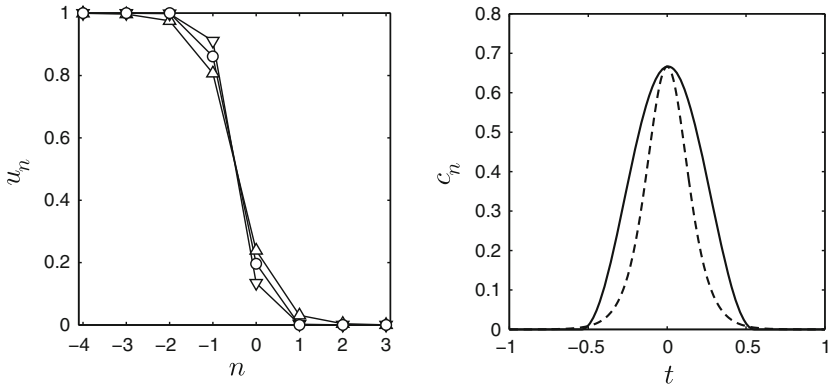


Fig. 3.5 *Left* Profiles of the displacements u_n for the sinusoidal magic mode (∘) and the ones given in the original supersonic crowdions paper by Kosevich and Kovalev (1973) [13]. For a quartic interatomic potential (Δ): $u_n = (2/\pi)\arctan[\exp(-q(n - Vt))]$ and for a cubic one (∇): $u_n = [1 + \exp(2q(n - Vt))]^{-1}$. *Right* Comparison of the compressions $c_n(t) = u_{n-1} - u_n$ for the magic mode (–) with the soliton for the continuous KdV equation [12]: $c_n = A\,\mathrm{sech}^2[q(n - Vt)]$ (- -). The functions have been rewritten so that the parameters have the same meaning. The magic mode is between the two K&K solutions and it is wider than the KdV one

As we have seen these equations are not as simple as they seem, due to the compactness condition for being nonzero. They look like harmonic waves, but they are not. The quantities in the equation have to be redefined but they keep the usual relationships for harmonic waves. In the following we propose operational definitions that are convenient but are only approximately correct, which is also natural at the fundamental ansatz is not exact either.

Velocity V	The average velocity of the kink. This is the magnitude best defined in numerical simulations and experiments.
Phase $\phi(n,t)$	Trivially, the phase of the bond n is $\phi(n,t) = \omega t - qn$. It determines when a bond is compressed $-\pi \leq \phi(n,t) < \pi$ and its state of compression. For example, $\phi(n,t) = 0$ is the phase of the state of maximum compression of the bond $c_n = A$, $\phi(n,t) = -\pi$ means the beginning of the compression process and $\phi(n,t) = \pi$ is the end. It is not periodic as a bond is just compressed once, if for example, $\phi_n = 2\pi$ $c_n = 0$ and not A.
Active	This term will change depending on the variable we refer to. For the phase it corresponds to $\phi(n,t) \in [-\pi, \pi)$.
Phase rate ω	It is the rate of variation of the phase with time or $\omega = \partial\phi(n,t)/\partial t = qV$. It is not the angular frequency as the ansatz is not a periodic function.
Compression time T	It is the interval of time for which a bond is compressed or activated, $T = 2\pi/\omega$. The interval of activity starts with zero compression $c_n = 0$ and finishes with the same value. In the meantime it achieves $c_n = A$, its maximum value. It also starts with $\phi = -\pi$ and finishes with $\phi = \pi$. As the numerical solutions become separate from the fundamental ansatz the operational definition of T is the value that brings about a better fit of v_n with the fundamental ansatz.
Phase delay q	It is the phase difference between two active (compressed) bonds n and $n-1$, that is, $q = \phi(n,t) - \phi(n-1,t)$. Alternatively, it can be defined as $q = 2\pi(\delta t/T) = \omega\delta t$, where δt is the time delay between two consecutive active bonds.
Kink length λ	It is the spatial extension of the kink, very much related with the number of active bonds at a given time λ/a or simply λ in scaled units. It is given by $\lambda = 2\pi/q$ and it is also the distance travelled by the kink during a time interval T, i.e., $\lambda = VT$. The

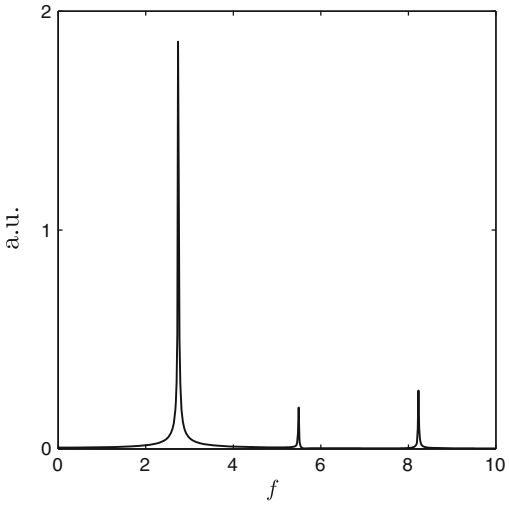


Fig. 3.6 Fourier spectrum of the kinetic energy of the supersonic crowdion obtained from numerical simulations. It is measured in a frame that moves with the crowdion in the lattice. We use arbitrary units for the intensity and scaled units (5 THz) for the frequency. The value of the first harmonic is exactly the characteristic linear frequency $\bar{\nu} = V_c/a = 2.7387$ and circular frequency $\bar{\omega} = 2\pi\bar{\nu} \simeq 17.2$, which corresponds to $\bar{\nu} \simeq 13.4$ THz in physical units

	usual relationships also hold, that is, $V = \omega/q$ and $\lambda = 2\pi/q$.
Amplitude A	It is the maximum value of the compression c_n.
Minimum distance R	It is the minimum value of the interparticle distance d_n, that is, $R = a - A$ or $R = 1 - A$ in scaled units.
Characteristic frequency $\bar{\nu}$	This is the inverse of the time δt that the kink needs to travel a distance of a lattice site, i.e. $\bar{\nu} = 1/\delta t = V/a$ or simply $\bar{\nu} = V$ in scaled units. Note that $\bar{\nu} = (\lambda/a)(1/T)$ (and *not* $1/T$). As the kink is not periodic it is the physical frequency at which the compression, the kinetic or potential energy or other magnitudes change while the kink travels in a lattice with period a. An example can be seen in Fig. 3.6. Their values for the crowdion are therefore $\bar{\nu} = 2.7387$ and $\bar{\omega} = 2\pi\bar{\nu} \simeq 17.2$, corresponding to $\bar{\nu} \simeq 13.4$ THz.

The equations for the displacements u_n and its derivatives will be seen in the following subsection.

3.3.3 Phasors for the Magic Mode

The easiest way to visualize the relative phases and distances of the variables is to consider the rotating complex vectors or *phasors*

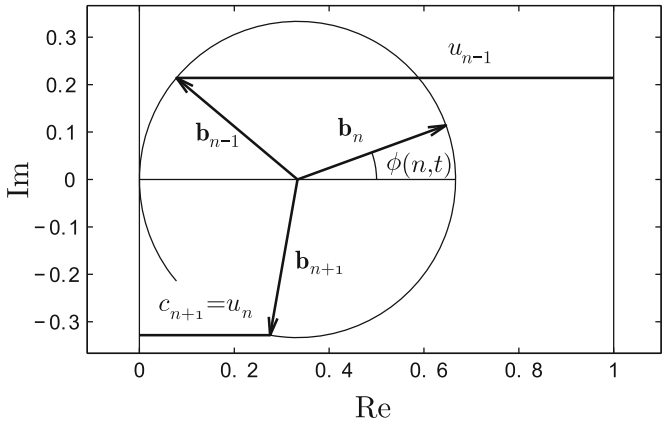


Fig. 3.7 Visualization of the evolution of the compressions $c_n = -v_n = u_{n-1} - u_n$ for the magic mode $q = 2\pi/3$ ($A = 2/3$). Three phasors $\mathbf{b}_{n-1}, \mathbf{b}_n, \mathbf{b}_{n+1}$ centered at $(0, A/2)$ and rotating anti-clockwise are *active* (the bonds are compressed) at a given time t when $-\pi \leq \phi(n,t) < \pi$. Their horizontal coordinates give the compression as can be seen with c_{n+1}. The maximum compression A is achieved for $\phi(n,t) = 0$. At $\phi(n,t) = \pi$, $\mathbf{b}_{n-1}$ will transform into $\mathbf{b}_{n+2}$ indicating that the bond $n-1$ is no longer compressed while the bond $n+1$ starts its compression cycle. The displacements are *active* while changing and only two are active at a given time $u_n = c_{n+1}$ and $u_{n-1} = c_n + c_{n+1} = 3A/2 - c_{n-1}$. For $m > n$, $u_m = 0$ and for $m < n-1$, $u_m = 1$. Also the nonzero velocities are $\dot{u}_n = -\omega\,\mathrm{Im}(\mathbf{b}_{n+1})$ and $\dot{u}_{n-1} = \omega\,\mathrm{Im}(\mathbf{b}_{n-1})$. Magnitudes are in lattice units $a = 5.19\,\text{Å}$

$$\mathbf{b}_n = \frac{A}{2}\mathrm{e}^{\mathrm{i}\phi(n,t)}, \quad \text{with} \quad \phi(n,t) = \omega t - qn \quad \text{and} \quad c_n = \frac{A}{2} + \mathrm{Re}(\mathbf{b}_n), \tag{3.7}$$

There is an important difference with the usual concept of phasors and it is that the circle is not periodic. The only phase interval where the phasors exists is $-\pi \leq \phi(n,t) < \pi$. If $\phi(n,t) < -\pi$ the phasor $\mathbf{b}_n$ has not yet come into existence and when $\phi(n,t) > \pi$, $\mathbf{b}_n$ has disappeared. Therefore, for $q = 2\pi/3$ at a given time there are three phasors in the unit circle as shown in Fig. 3.7. The three phasors have their origin at $(A/2, 0)$ and rotate anti-clockwise with angular speed ω while the time t increases, let us denote them $\mathbf{b}_{n-1}$, $\mathbf{b}_n$, $\mathbf{b}_{n+1}$. In the following n has to be understood as the index of the inner bond of the three compressed ones or the index of the intermediate phasor, that is $-\pi/3 \leq \phi(n,t) < \pi/3$. If we denote as $t_n = n/V$ the time for which $\phi(n,t_n) = 0$, then $-T/6 \leq t - t_n < T/6$. This is not a restriction as there is always a bond central to the three compressed ones.

The phasor $\mathbf{b}_{n+1}$ is behind $\mathbf{b}_n$ by an angle q and so on for a kink travelling to increasing n number. Note that $\mathbf{b}_{n-1} + \mathbf{b}_n + \mathbf{b}_{n+1} = 0$.

Therefore, the particles first reached by the kink have larger phase ϕ. The angle $\phi = \pi$ is the angle for change of number, that is, when $\mathbf{b}_{n-1}$ reaches that position it disappears from the circle and ceases to be active, indicating that the bond $n-1$

is no longer compressed. At the same time, a new phasor $\mathbf{b}_{n+2}$ appears at $\phi = -\pi$, indicating that a new bond has started to be compressed or becomes *active*, after a time T it will in turn become inactive. As shown in Fig. 3.7, the horizontal distance to the vertical straight line through the origin is the compression $c_n = A/2 + \mathrm{Re}(\mathbf{b}_n)$.

Let us now consider the displacements u_n, using $c_n = u_{n-1} - u_n$ or $u_{n-1} = u_n + c_n$. The particles not yet reached by the kink have zero displacement and the first nonzero compression is c_{n+1}. Therefore $u_n = c_{n+1}$ and $u_{n-1} = u_n + c_n = c_n + c_{n+1} = A + \mathrm{Re}(\mathbf{b}_n + \mathbf{b}_{n+1}) = A + \mathrm{Re}(-\mathbf{b}_{n-1}) = 3A/2 - c_{n-1}$ as represented in Fig. 3.7. To summarize

$$u_{n+1} = 0 \tag{3.8}$$

$$u_n = c_{n+1} = \frac{A}{2} + \mathrm{Re}(\mathbf{b}_{n+1}) = \frac{A}{2} + \frac{A}{2}\cos(\omega t - q)$$

$$u_{n-1} = \frac{3A}{2} - c_{n-1} = A - \mathrm{Re}(\mathbf{b}_{n-1}) = A - \frac{A}{2}\cos(\omega t + q). \tag{3.9}$$

These equations are valid for $t = 0$ chosen as the time for which the central bond n is most compressed $c_n = A$ and remains central, $-\pi/3 \le \phi(n,t) < \pi/3$ and $-T/6 \le t < T/6$. The following displacement $u_{n-2} = c_{n-1} + c_n + c_{n+1} = 3A/2 = 1$ and equally $u_m = 1$ for $m \le n-1$, that is, for the particles that have been left displaced by a lattice unit after the passage of the kink.

The particle velocities $\dot{u}_m = \partial u_m/\partial t$ can also be calculated and visualized easily using $\dot{\mathbf{b}}_m = \mathrm{i}\omega\mathbf{b}_m$ and therefore $\mathrm{Re}(\dot{\mathbf{b}}_m) = -\omega\mathrm{Im}(\mathbf{b}_m)$

$$\dot{u}_n = \dot{c}_{n+1} = -\omega\,\mathrm{Im}(\mathbf{b}_{n+1}) = -\omega\frac{A}{2}\sin(\omega t - q)$$

$$\dot{u}_{n-1} = -\dot{c}_{n-1} = \omega\,\mathrm{Im}(\mathbf{b}_{n-1}) = \omega\frac{A}{2}\sin(\omega t + q). \tag{3.10}$$

For any other m, $\dot{u}_m = 0$.

For other integer values of $\lambda = 2\pi/q$, there are λ active phasors and for non integer values, the number of active phasors changes between the two integers below and above λ. However, in this chapter we will concentrate on the *magic* mode $q = 2\pi/3$ as it is very close to the crowdion found in the simulations.

In this way it is easy to construct the evolution of the particles during the compression time T as can be seen in Fig. 3.8 for six times between $-T/2$ to $T/2$. In this time the crowdion advances a length $\lambda = 3$, that is, three lattice units, but a single particle just travels a single lattice unit. Therefore the average velocity of a particle $\langle V_p \rangle$ is three times smaller than the crowdion velocity V_c. It is worth mentioning that Fig. 3.8 also shows that only the two particles participating in the kink motion are mostly involved in the motion at the same time, as the fundamental ansatz with sinusoidal waveform, 3.5, with $q = 2\pi/3$ predicts [14, 15].

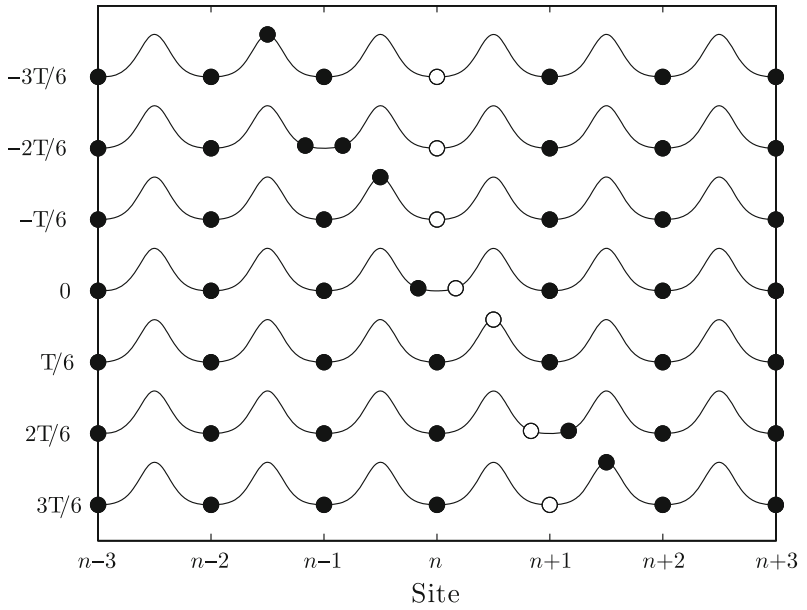


Fig. 3.8 Magic mode $q = 2\pi/3$ for a kink. A sketch of the system is shown for a full time of compression T at time intervals $T/6$. The white particle is labelled n, therefore its displacement is u_n and the bond at its left is also bond n with compression $c_n = -v_n = u_{n-1} - u_n$. The origin of time has been taken as the time of maximum compression of bond n, i.e., $c_n = A$ and $d_n = a - A$. During the time interval in the graph the white particle n moves from site n to site $n + 1$. At time $t = -T/2 = -3T/6$, the bond n is uncompressed ($c_n = 0$, $d_n = 1$) and again becomes uncompressed at $t = 3T/6 = T/2$. Note that during the first two $T/6$ intervals, although the bond d_n is changing, there is no appreciable displacement u_n. Note also, that the compressed structure at $t = -3T/6$ between sites $n - 2$, $n - 1$ has moved at $t = 3T/6$ to sites $n + 1$, $n + 2$, i.e., the kink has moved three sites or the length of the kink $\lambda = V_c T$, while the white particle n has moved a single site. Therefore, the average velocity of a particle in a time T is $\langle V_p \rangle = 1/T = V_c/3$. The average velocity of a particle for the following four $T/6$ intervals, when it is actually moving, is $\langle V_p \rangle' = 1/(2T/3) = V_c/2$

3.4 Kinks with Substrate Potential: The Crowdion

The introduction of a substrate potential also modifies substantially the behaviour of the particles in the kink. The phase $\phi(n, t)$ is still very useful for the interpretation of the movement of the particles. The crowdion, of ultradiscrete kink of fixed velocity and energy that appears in the simulations corresponds basically to the *magic mode* but with some differences. Considering the white ball in Fig. 3.8 and denoting it by n, it basically does not move from $t \in [-3T/6, -T/6]$ as the Coulomb repulsion from particle $n - 1$ is weak. For times close to $t = 0$ when the strong ZBL potential acts, it receives most of its momentum which it will transfer in due course to the following particle $n + 1$. However, in between, it will have to overcome the barrier of the potential, experiencing a deceleration and afterwards an acceleration while

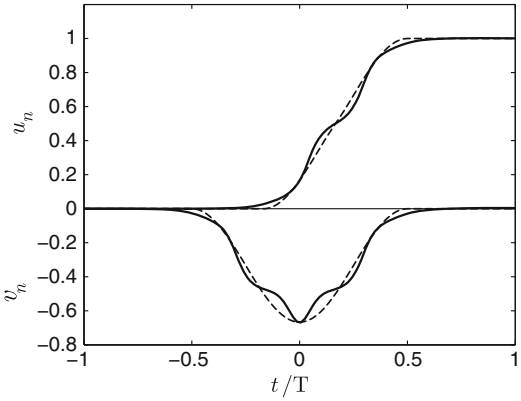


Fig. 3.9 Comparison of the ultradiscrete kink defined with the fundamental ansatz in 3.5 with $A = 2/3$ and $q = 2\pi/3$ with the ultradiscrete kink with fixed velocity obtained in the simulations dubbed *crowdion* in this chapter. *Dashed lines* Ansatz, *continuous lines* Crowdion. The displacements u_n correspond to the *upper curves* while the strains $v_n = u_n - u_{n-1}$ correspond to the *lower curve*. The kink transforms into a double kink because the displacement between two equilibrium sites is divided by the nonequilibrium position at the top of the potential well as can be seen in Fig. 3.8. The magnitudes u_n and v_n are given in lattice units $a = 5.19$ Å. The compression time is given by $T = 1.095$ or 0.22 ps in physical units

going downhill. Eventually the acceleration becomes negative as it experiences the ZBL repulsion from the particle $n + 1$ ahead. The ascending and descending of the potential barrier by the particle produces a remarkable change in the particle displacement u_n and strain $v_n = u_n - u_{n+1}$ as shown in Fig. 3.9. The kink has been converted into a double kink: the first kink corresponds to the translation of a particle from the well bottom to the top of the nearest potential barrier and the second kink to the subsequent displacement to the following well bottom.

We would also like to mention in connection with Fig. 3.9, that the fundamental ansatz with sinusoidal waveform (3.5) for $q = 2\pi/3$, and corresponding dashed lines in these figures gives much better agreement with the simulations of supersonic kink motion in the Fermi-Pasta-Ulam lattice without substrate [15]. The deviation from the ansatz prediction in Fig. 3.9 is caused only by the presence of the substrate because the ansatz was originally proposed for the translationally-invariant Fermi-Pasta-Ulam lattice [14, 15].

The separation from the ideal functions of the ansatz can also be seen in Fig. 3.10 where the displacements are shown at a given time. It can be observed that the deviation from the magic mode are important qualitatively but not so much quantitatively. A more significant difference appears in the velocities which are represented in [3] but can also be seen easily in the slope of Fig. 3.9. According to (3.10) the maximum particle velocity using the ansatz is $\omega A/2 = 1.91$ or 5 km/s, while for the observed one for the crowdion it is 2.9 in scaled units or 7.6 km/s attained when the particle is going uphill or downhill. The minimum particle velocity is achieved at the top of the barrier.

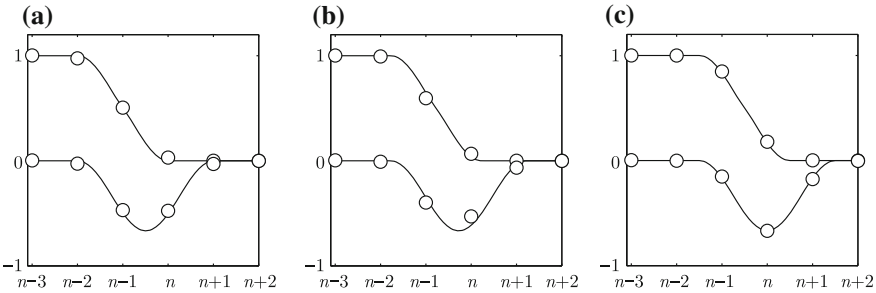


Fig. 3.10 Three plots at different times **a** $t \simeq -T/6$ **b** $t \simeq -0.5T/6$ **c** $t \simeq 0$. They show the profile of the displacements u_n (*upper curves*) and strains $v_n = u_n - u_{n-1}$ (*lower curves*) with respect to the particle and bond index n. The *continuous lines* represent the theoretical ansatz (3.5) and the *circles* represent the points corresponding to the numerical simulation of the crowdion. Time $t = 0$ corresponds to the maximum compression of bond n. The variables u_n and v_n are given in lattice units $a = 5.19\,\text{Å}$. Every $T/6$ the theoretical and numerical solutions becomes almost identical as can also be seen in Fig. 3.9. Subfigure (**b**) represents the maximum separation from the theoretical curves

3.5 Phonons and Crowdions

The introduction of the substrate potential brings about significant changes in the system, not only for the kinks but also for the phonon spectrum. We first review the properties of phonons in a system with substrate potential and then use them to analyze the phonon tail of the crowdion.

3.5.1 Phonons in Presence of a Substrate Potential

The dynamical equations for small perturbations become

$$\ddot{u}_n = -\omega_0^2 u_n + c_s^2(u_{n+1} + u_{n-1} - 2\,u_n), \tag{3.11}$$

with $c_s = \sqrt{2}$. The linearization of the coupling terms comes only from the Coulomb one. The ZBL potential does not appear because it is zero for small oscillations. The substrate potential has been reduced to a harmonic one expanding the sinusoidal functions. The value of ω_0 is obtained using the values of the Fourier coefficients of the substrate potential in (3.4)

$$\omega_0^2 = -\sum_{m=1}^{4} (2\pi m)^2 U_m. \tag{3.12}$$

The resulting numerical value is $\omega_0 = 4.48$ in scaled units, corresponding to 3.6 THz or 119 cm^{-1}. The coefficient $c_s = \sqrt{2}$ or 3.7 km/s in physical units is the speed of sound in the system without substrate.

Substitution of $u_n = \exp(\mathrm{i}(qn - \omega t))$ leads to

$$-\omega^2 = -\omega_0^2 + c_s^2(\mathrm{e}^{\mathrm{i}q} + \mathrm{e}^{-\mathrm{i}q} - 2). \tag{3.13}$$

From this equation it is easy to obtain the phonon spectrum, the phonon velocities and the group phonon velocities. They are given by

$$\omega^2 = \omega_0^2 + 4\,c_s^2 \sin^2\left(\frac{q}{2}\right); \quad V_{\text{phase}} = \frac{\omega}{q}$$
$$V_g = \frac{\mathrm{d}\omega}{\mathrm{d}q} = \frac{c_s^2 \sin q}{\sqrt{\omega_0^2 + 4\,c_s^2 \sin^2(\frac{q}{2})}}. \tag{3.14}$$

The corresponding equations for the system without substrate are identical with $\omega_0 = 0$. In this case c_s is both the phase and group velocity in the long-wavelength limit ($q \to 0$).

For the system with substrate ω_0 is the lowest phonon frequency, corresponding to the long wavelength limit ($q \to 0$). This can be seen in Fig. 3.11 where the dispersion relation, the phase and the group velocities are shown. Note the main changes produced by the introduction of the substrate potential: (a) the phonon spectrum becomes optical, i.e., bounded from below, (b) the phase velocity diverges when $q \to 0$, and (c) the group velocity becomes zero both at $q = 0$ and $q = \pi$ and has a maximum close to $q = \pi/2$ but with a much lower velocity.

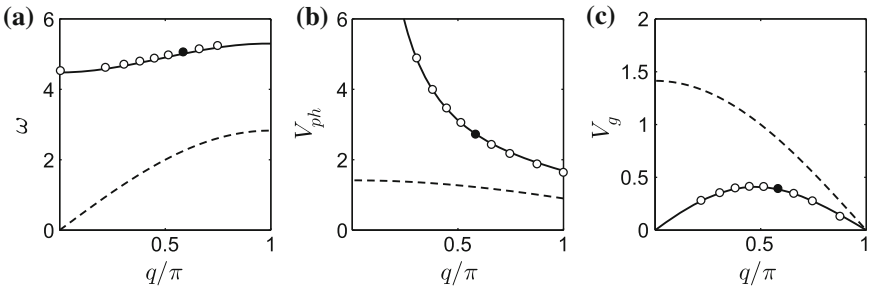


Fig. 3.11 **a** Dispersion relation, **b** phase velocity and **c** group velocity. The three plots are for longitudinal phonons in a potassium row for the system without substrate (*dashed line*) and with substrate (*continuous line*). Scaled units are approximately 5 THz for frequency and 2.6 km/s for velocities. *White circles* are measurements from different numerical simulations. The *black circles* are the theoretical values for the phonon tail obtained by making the phonon phase velocity equal to the crowdion velocity

The value of the wavevector q corresponding to the maximum group velocity can be calculated as it corresponds to $\mathrm{d}V_g/\mathrm{d}q = 0$. Equivalently it corresponds to the maximum of the function

$$f(q) = \frac{V_g^2}{c^4} = \frac{\sin^2(q)}{\omega_0^2 + 2c_s^2(1 - \cos(q))}, \tag{3.15}$$

where we have used that $2\sin^2(q/2) = 1 - \cos(q)$. Then

$$\frac{\mathrm{d}f(q)}{\mathrm{d}q} = \frac{2\sin(q)\cos(q)[\omega_0^2 + 2c_s^2 - 2c_s^2\cos(q)] - \sin^2(q)[2c_s^2\sin(q)]}{\omega_0^2 + 2c_s^2 - 2c_s^2\cos(q)}. \tag{3.16}$$

Making the numerator equal to zero, we obtain:

$$(\omega_0^2 + 2c_s^2)\cos(q) - 2c_s^2\cos^2(q) - c_s^2\sin^2(q) = 0, \tag{3.17}$$

which leads to a second order equation in $\cos(q)$

$$c_s^2\cos^2(q) - (\omega_0^2 + 2c_s^2)\cos(q) + c_s^2 = 0, \tag{3.18}$$

with solution

$$\cos(q) = \frac{\omega_0^2 + 2c_s^2 \pm \sqrt{\omega_0^4 + 4\omega_0^2 c_s^2}}{2c_s^2}. \tag{3.19}$$

For the values in the present system, only the minus sign gives a real value of $q = 1.4870\,\mathrm{rad}$ corresponding to a wavelength $\lambda = 4.2253$, and maximum group velocity $V_{g,M} = 0.4091$.

3.5.2 Crowdion Phonon Tail

When the kink is produced, its amplitude diminishes towards the crowdion's one in an asymptotic way. Therefore after some time, the nonlinear waves are no longer produced but there is always a linear vibration left behind although with decreasingly smaller amplitude. This is why the crowdion continues propagating. The tail is a plane wave and as such does not transport energy, but theoretically could be measured to detect crowdion properties. We will call it the *phonon tail*. Note that the velocity to describe these plane waves is the phase velocity and which in this case is unbounded. The crowdion is moving at speed V_c and leaves at each site some small perturbation exactly at the same estate at times separated by $\delta t = 1/Vc$. In other words, the phase velocity of the phonon tail V is the same as the velocity of the crowdion V_c.

$$V_{\mathrm{phase}} = V_c = 2.7387 \quad (7.2\,\mathrm{km/s}) \quad \text{(Phonon tail)}. \tag{3.20}$$

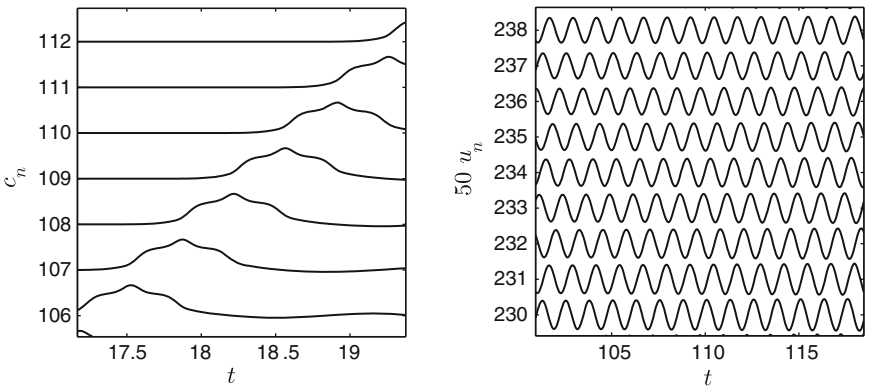


Fig. 3.12 *Left* Plot of $c_n + n$ where the double soliton structure, period and other crowdion parameters can be appreciated. *Right* Phonon tail amplified 50 times. It is a perfect plane wave with parameters with the same velocity of the crowdion $V = V_c$ and similar parameters although not identical $T \gtrsim T_c, q \gtrsim q_c, \lambda \gtrsim \lambda_c$. Note that this parameters are not well defined for the crowdion and only approximate

The wave number of the tail can be obtained from the equation $V_{\text{phase}} = V_c = w/q = [\omega_0^2 + 4\sin^2(q/2)]^{1/2}/q$, which can be solved numerically or graphically from Fig. 3.11b. The result is $q = 1.8290 = 0.5822\pi$ and therefore $\omega = qV_c = 5.00$, $T = 2\pi/\omega = 1.2544$ and $\lambda = 2\pi/q = 3.44$. So the parameters are very close to the ω_c, T_c and λ_c of the crowdion. In some sense, they can be considered as the actual parameters of the crowdion as they can be measured. Note that these parameters, as λ_c are not well defined as they depend on the algorithm used to fit the numerical solutions. Figure 3.12 represents a picture of c_n and a view of the phonon tail for u_n, similar to c_n where the perfect plane wave and its parameters can be appreciated.

3.6 Some Numerical Simulations with Ultradiscrete Kinks or Crowdions

In this section we present the results of different simulations to show the capacity of the crowdions to survive a perturbed environment when larger energy is initially delivered and, second, the behaviour of the crowdions with temperature.

3.6.1 Excess Energy

We present some examples of simulations when the lattice is given more energy than the 26.2 eV needed to produce the supersonic crowdion. The energies range from 130 to 520 eV. They are represented in Fig. 3.13. In (a) a single crowdion is formed

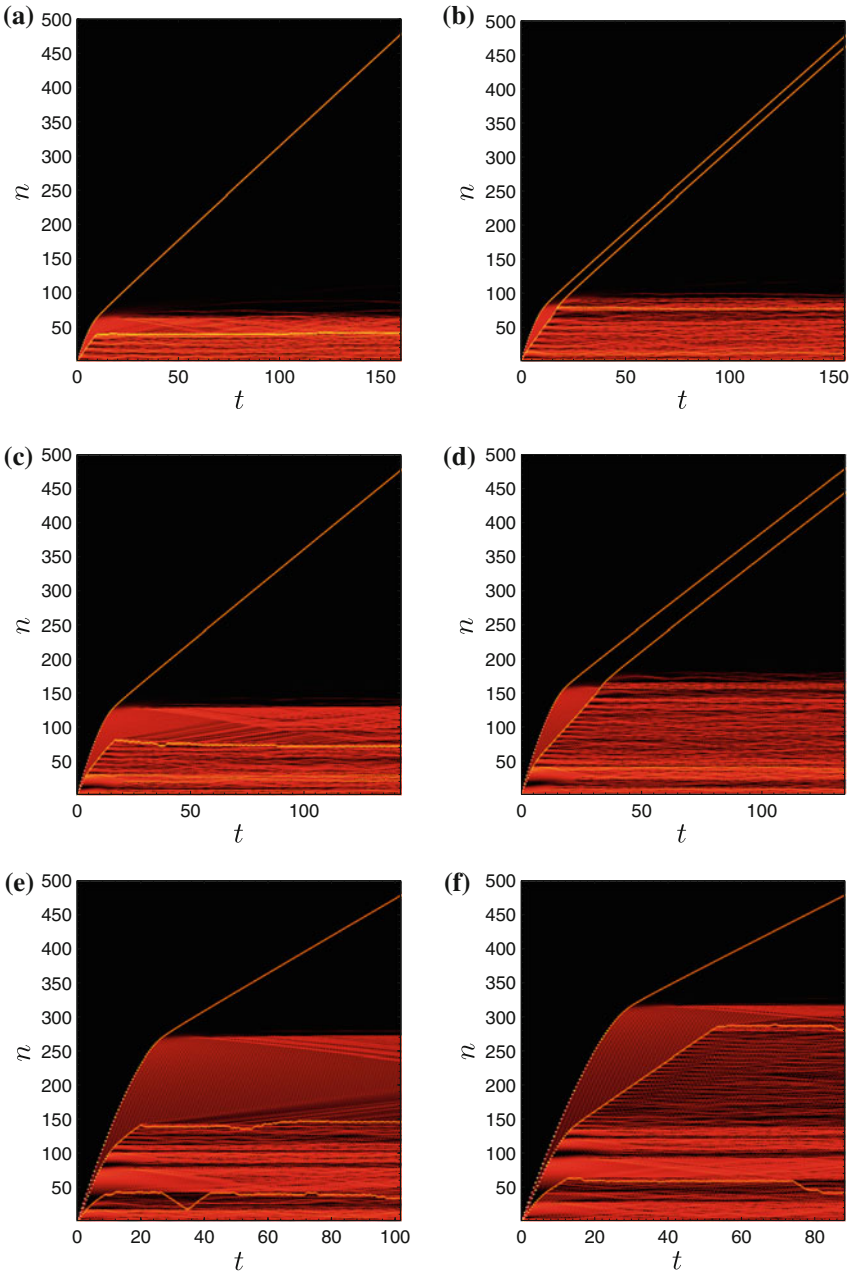


Fig. 3.13 *Color* Particle energy plots of several examples of crowdion formation in arbitrary units of $\simeq 3\,\text{eV}$. Initial energy increases form **a** to **f**. Many features can be observed, among them the specific velocity of the crowdion V_c, the formation of nonlinear waves and phonons, the formation of two crowdions and the survival of the crowdion in the severely perturbed media for hundreds of sites. **a** $E_0 = 130.1\,\text{eV}$, **b** $E_0 = 159.3\,\text{eV}$, **c** $E_0 = 229\,\text{eV}$, **d** $E_0 = 268.1\,\text{eV}$, **e** $E_0 = 453.5\,\text{eV}$, **f** $E_0 = 515.7\,\text{eV}$

after nonlinear waves are emitted. In (b) two crowdions are formed leaving behind an stationary linear wave. Note how the second crowdion survives to the tail of the first and the common velocity V_c of both. In (c) the excessive energy destroys the second crowdion which transforms into a highly localized nonlinear stationary wave. In (d) the second crowdion survives again, while in (e) it is again destroyed. Extensive phonon radiation and wandering kinks can be seen in the latter figure. In (f) a second crowdion survives for 150 sites in a highly perturbed media but it is finally pinned down.

3.6.2 Thermalized Medium

An interesting question is whether the crowdion can travel trough a previously thermalized medium. This is not only a question of general interest but particulary important for mica muscovite. As it has been calculated in the chapter *Tracks in mica: 50 years later* in this book [27], the recording process of tracks happens a few kilometers underground under large pressure and temperatures of 700–1000 K. Although much more work is necessary, the answer is positive. For comparison Fig. 3.14a, b shows two simulations at 300 and 1000 K in the system without substrate potential where the kink survives over hundreds of lattice sites. It is not really surprising as, if we compare the energy of the crowdion 26.2 eV with the mean thermal energy of a particle k_BT, the crowdion energy is 1000 and 300 times larger at 300 and 1000 K, respectively.

In the case of including the substrate potential, as shown in Fig. 3.14c, d for 300 and 1000 K respectively, the crowdion can also travel for hundreds of sites of the previously thermalized media. As it was studied in [3], the crowdion always has finite kinetic energy, but the final total energy of the kink, E_k, is always of the order of magnitude of the Peierls-Nabarro (PN) barrier. The equivalent kinetic energy equivalent for the thermalized media is 0.005 (0.013 eV) at 300 K and 0.016 (0.043 eV) at 1000 K in normalized and physical units. These values are far below the energy difference between the PN barrier and the kink energy. However, in some simulations, for temperatures of 1000 K the thermalization is not completely achieved due to appearance of nonlinear waves instead of phonons. Therefore, localized peaks of the background vibrations can interfere with the crowdion where, in some cases, it can be trapped leading to a highly localized nonlinear stationary perturbation. Figure 3.14d shows and example of this situation, where the crowdion is eventually trapped forming an interstitial defect.

Thermal effects discussed in this section lead to different survival path lengths of the crowdions. If the hypothesis of crowdions propagating in mica muscovite is correct, they might be related with some of the tracks observed in the mineral. Other feature of the presented simulations worth remarking on is that the high equivalent temperature of the nonlinear tail radiation of the crowdion is likely to favour a change of structure and the formation of tracks.

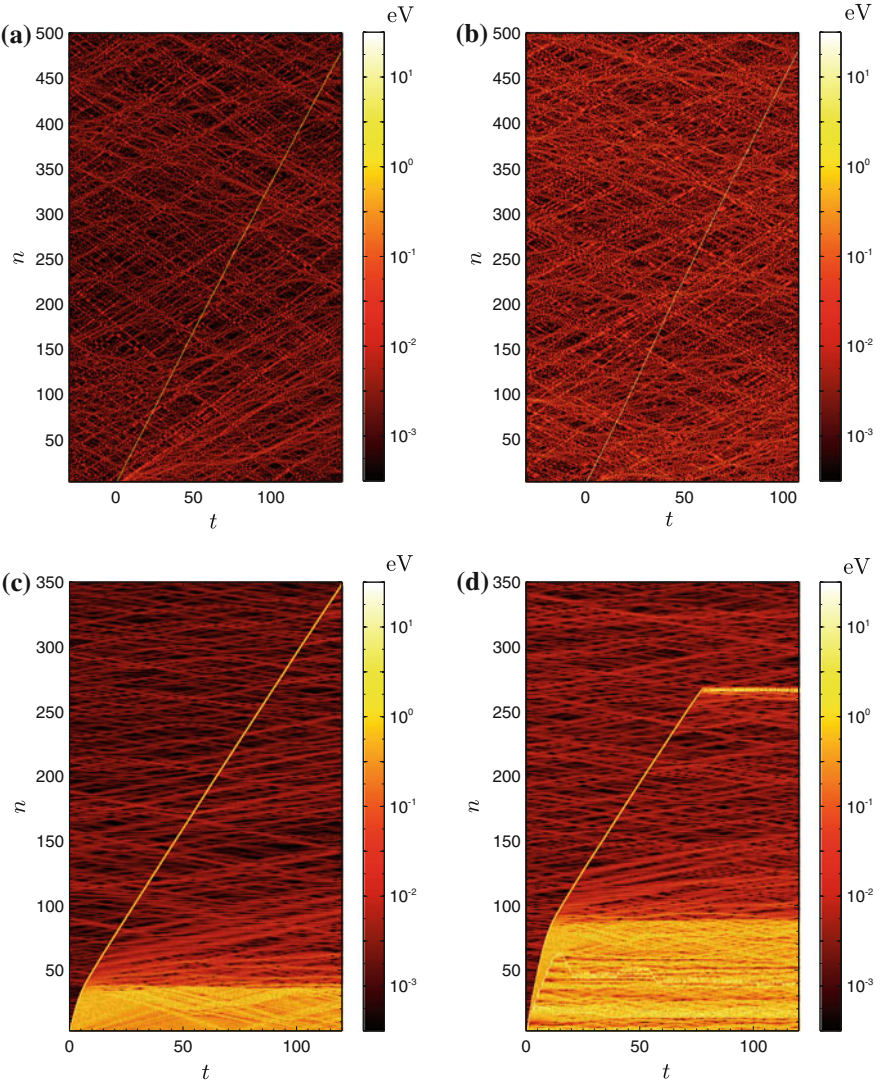


Fig. 3.14 *Color* Particle energy plots of two crowdions travelling in a previously thermalized medium at **a**, **c** 300 K and **b**, **d** 1000 K, *top* without and *bottom* with substrate potential. *Color bars* are in $10 \log_{10}(E)$ units

3.7 Recoil Energy of ^{40}K

If the hypothesis of quodons being vibrational entities of ions of potassium is correct, the most likely source of energy is the recoil from ^{40}K because (a) the energy will be given directly to the potassium ion K^+, (b) the relative abundance and decay frequency of ^{40}K, and (c) because of the energies involved as explained below.

The two most abundant isotopes of potassium are the stable ^{39}K and ^{41}K isotopes, with 93.7 and 6.7 % abundance respectively. The next most abundant isotope is ^{40}K with a very long half life of 1.248×10^9 years and abundance of 0.0117 %. This isotope is the most important source of radioactivity for humans.

As shown in Fig. 3.15 and Table 3.2, the nucleus ^{40}K experiences decay through different branches with two daughter nuclei ^{40}Ca and ^{40}Ar [4, 20]. The main parameters of the decay are I, the intensity of a given branch in % and Q, which is the difference between the rest masses of the parent and daughter *atoms*. The difference of mass between atoms is better tabulated than between nuclei. As the atoms are neutral the mass difference between nuclei has to take into account the difference in the number of electrons in the neutral atoms. The available energy will depend on the rest mass of the parent and daughter nuclei and other particles. It will be obtained below for each type of decay.

The decay branches, $\beta-$ and $\beta+$ involve the emission of an electron or a positron and a neutrino. The electron or positron velocities are such that they have to be treated relativistically, while the recoil velocity of the much heavier nuclei can be described classically. We will suppose an electron to simplify the language, but a positron can

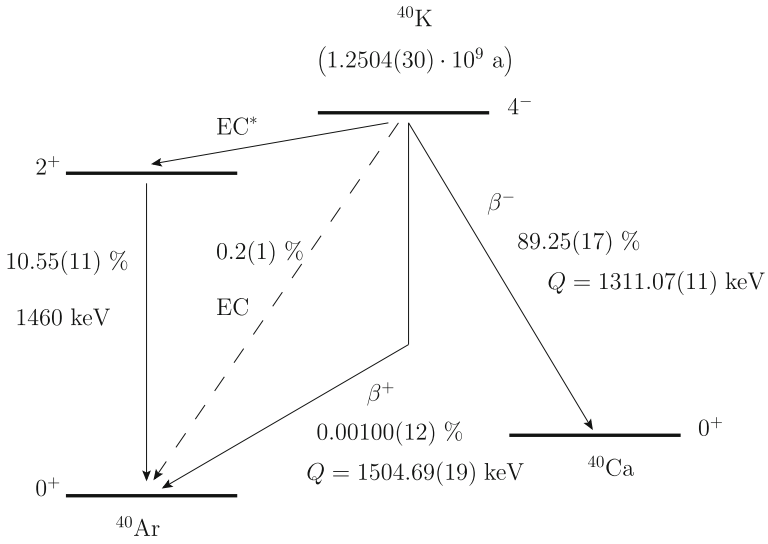


Fig. 3.15 Sketch showing the different decays and branching of ^{40}K. Reproduced with permission from [21]. Copyright Creative Commons BY 3.0

Table 3.1 Table of ionization energies (eV) of daughter atoms from ^{40}K decay [17]

Element	I	II	III	IV	V
Ar	15.76	27.63	40.74	59.81	75.02
K	4.34	31.63	45.81	60.91	82.66
Ca	6.11	11.87	50.91	67.27	84.50

be equally described in what follows. The maximum recoil energy of the nucleus is obtained when the neutrino gets no kinetic energy. The recoil energy is much smaller than the electron energy, so it can be neglected in the energy calculations while due to its large mass, it is essential for the momenta balance. The electron maximum energy is $E_e = m_e\, c^2 + E$, being E the available energy in the decay, and $E_e^2 = m_e^2\, c^4 + p_e^2 c^2$, where p_e is the momentum of the electron. Considering the parent nucleus at rest, the momentum of the nucleus is identical to the momentum of the electron $p_N = p_e = (1/c)(E_e^2 - m_e^2 c^4)^{1/2}$ and the maximum nucleus recoil energy is given by $E_N = p_N^2/(2m_N)$. The decays always involve the emission of a neutrino and may include the emission of a photon, either γ from the nucleus of X from the electron shell, although the latter have much smaller energy and momentum and will be of no importance for K^+ recoil. The neutrino can be considered as a massless particle as its rest mass it known to be below 2.2 eV/c^2. Therefore for photons or neutrinos their energy is given by $E_{\nu,\gamma,X} = pc$. If only a photon or a neutrino is emitted the recoil momentum p_N is equal to the momentum of the photon or neutrino and trivially $E_N = {P_N}^2/(2\, m_N)$. If there are only two daughter particles the recoil energy E_N has a single value.

Other data of interest are the ionization energies of K and of the daughter nuclei. If the recoil energy is larger than the ionization energy of the atoms that interact, it can be used to ionize an atom or ion and the energy cannot be transferred to the neighbours. The ionization energies of the daughter atoms from ^{40}K decay can be seen in Table 3.1. A examination of the possible ionization processes is done in the following subsection.

As the lattice is formed by K^+, it is probable that the second ionization of K, 31.6 eV, is an upper limit for crowdions or single row kink energies.

3.7.1 ^{40}K Decay Branches

Here, we analyze in detail the different decay branches. A summary if presented in Table 3.2 and a sketch in Fig. 3.15.

The ^{40}K decay branch that leads to ^{40}Ca is:

β^-: *Decay with emission of an electron.*

With $I\beta^- = 89.25\,\%$ and mass difference between atoms $Q = 1311.07$ keV [20].

As the Ca atom has an extra electron, discarding the electron binding energy

Table 3.2 Table of decays for ^{40}K

Decay	β^-	EC1	EC1+CE[a]	EC2[b]	β^+
Intensity (%)	89.25	10.55	0.001	0.2	0.001
T (keV)	1311.07	1460	1460	1504.69	483.7
Emitted charged particle	e^-		e^-	e^-	e^+
Recoil from	ν+e^-	γ	e^-	ν	ν+e^+
Max Recoil (eV)	42	29.2^M	49.7^M	31.1^M	10
Daugther ion (A = 40)	Ca^{++}	Ar^+	Ar^{++}	Ar^{++}	Ar
Max V (Km/s)	14.4	12^M	15.7^M	12.2^M	7
Ionization of daughter (eV)	50.6	27.7	40.8	40.8	15.8
Δq (e)	+1	0	+1	+1	−1

[a]Subset of EC1 when the gamma is delivered to a shell electron; ^{M} Monocromatic
[b]Direct decay to Ar ground state, recoil from neutrino emission; 3 KeV Auger e^-
EC Electron capture; *CE* Conversion electron; *T* Energy available excluding rest masses
Ionization energy of K^+ 31.6 eV

of a few keV, the mass difference between nuclei is $Q + m_e c^2$ and the energy available when emitting an electron is $E \simeq Q + m_e c^2 - m_e c^2 \simeq Q$ which will be shared between the electron and the antineutrino emitted. Therefore, the maximum kinetic energy of the electron or *endpoint* is almost equal to Q. The daughter nuclei of ^{40}Ca have a continuous distribution of energy with a maximum of $E_k = 42$ eV at the endpoint corresponding to a velocity $V = 14.4$ km/s.

The proton number increases by one, but the number of electrons does not change, therefore the daughter ion would be Ca^{++} with 50.6 eV third ionization energy. This is a likely origin of quodons for the decays with recoil energy smaller than the 31.6 eV K second ionization energy. The recoils with larger energy will be able to deliver up to 10.4 eV after the first collision that could produce breathers but not crowdions.

The following processes have ^{40}Ar as daughter nuclei being the difference between the *atomic* masses $Q = 1504.69$ keV. As the Ar atom has an electron less than K, discarding the electron binding energies the mass difference between nuclei is $\simeq Q - m_e c^2$ and the energy available depends on the specific decay.

EC1: *Electron capture with decay to* ^{40}Ar *excited state and* γ *radiation.*
With $I\varepsilon = 10.55$ %, an electron from the shell is captured, therefore the available energy is $E \simeq Q - m_e c^2 + m_e c^2 \simeq Q$. In this decay a monoenergetic neutrino of 44 keV is emitted with negligible recoil (26 meV) and the daughter nucleus is in an excited state. Thereafter, the excited nucleus decays to the ground state with the emission of a 1460 keV γ ray [20]. The corresponding K^+ recoil energy of

^{40}Ar is $E_k \simeq 29.2$ eV with velocity $V = 12.0$ km/s. As this is a two body process E_k has only slight variations due to interactions with the shell electrons.

As no charge is emitted from the ion K^+, the daughter will also be a monovalent ion of Ar^+, with 27.7 eV second ionization energy. So there is some probability that the first Ar^+ collision with K^+ will further ionize Ar^+. The remaining energy 1.3 eV will not be enough to produce a kink but may produce a breather.

EC1+CE: *Electron capture with decay to* ^{40}Ar *excited state and conversion electron.* This is actually a subset of the previous decay, but with a probability I = 0.001 per 100 decays, the 1460 keV γ ray emitted can interact with the shell and deliver the energy to an electron, called a conversion electron. Save for a few keV of binding energy the γ energy is converted into kinetic energy of the electron, with a recoil for the ion of 49.7 eV and 15.6 km/s. This is the largest energy of all the recoils. As an electron has been emitted from the shell, the daughter ion will be Ar^{++} with 40.8 eV third ionization energy. This ionization and the 31.6 eV second one of K^+ are likely to occur. The remaining energies of 8.8 or 18 eV cannot produce a crowdion but will be able to produce breathers.

EC2: *Electron capture with direct decay to* ^{40}Ar *ground state*.
With probability $I = 0.2\,\%$, the energy available as in the decay above is $E \simeq Q = 1504.69$. There is a direct decay to the ground state of ^{40}Ar after the capture of a shell electron and the emission of a monoenergetic neutrino that takes most of the energy available $E \simeq 1504.69$ keV minus the electron binding energy which is only a few keV [21, 34]. The recoil energy is 31.1 eV. The shell emits a 3 keV Auger electron when another electron of the shell occupies the vacancy left by the captured electron, however, this has a negligible recoil.

The daughter nucleus has lost a positive unit charge but also the shell has lost two electrons, the captured one plus the Auger electron. Therefore the daughter ion will be Ar^{++}, which has too little energy for further ionization of Ar^{++} or K^+ which need 40.8 and 31.6 eV, respectively. Therefore, it would be a likely source of crowdions but difficult to distinguish from the β^- recoil.

β^+: *decay with positron emission.*
With very low probability $I\beta^+ = 0.001\,\%$, the available energy is the mass difference between nuclei minus the mass energy of the positron emitted, that is, $E \simeq Q - m_e c^2 - m_e c^2 = Q - 2m_e c^2 = 483.7$ keV. The energy E is shared between a neutrino, the emitted positron and the daughter nucleus. Therefore, the positrons have a continuum of energies with a maximum one or endpoint 483.7 keV [4, 8, 20], which leads to the maximum recoil energy $E_k \simeq 10$ eV and velocity of 7 km/s.

As the atomic number is decreased by one unit to $Z - 1$, the initial ion K^+ has lost a positive unit charge, but there has been no change in the number of electrons, thus the daughter ion will be a neutral Ar interacting with short range forces with the neighbouring K^+. The first ionization energy of Ar is 15.8 eV, so, actually, the Ar atom has less of the required energy for ionizing itself or for further ionization of K^+ and will be able to keep the 10 eV energy. This seems too

little to produce a kink but may produce a breather. Due to their positive charge, positrons leave tracks in mica muscovite [25, 35].

A study with the correlation of positron tracks, thickness distribution of quodon tracks and other characteristics could make it possible to confirm the nature and characteristics of quodons. See chapter *Tracks in mica, 50 years later* in this book for more details [27].

3.7.2 Secondary Processes

Electron–positron pair production:

This is a secondary process after the γ ray emission of 1460.82 keV considered above [8]. It needs the interaction of the γ ray with a nucleus, and the produced positron and electron can share the energy in any proportion. The maximum recoil energy corresponds to a single particle taking almost all the energy except for the small amount taken by the nucleus, which is necessary due to momentum conservation. The available kinetic energy is $E = E_\gamma - 2\,m_e\,c^2 = 437.4\,\text{keV}$ and the maximum recoil energy is $E_k = 8.8\,\text{eV}$. The probability of the combined process of electron capture and pair production is of the same order of magnitude as β^+ emission and also the energies are similar [8]. The probability of interaction of the γ ray with a nucleus is proportional to Z^2 which favors the interaction with potassium; however, potassium atoms are only 5 % of the atoms in mica.

As the energy is smaller than the second ionization energy of K of 31.6 eV it is likely that the subsequent K^+–K^+ collisions are elastic.

Other secondary processes may also occur via other radioactive nuclei and their corresponding decay, but it will be beyond the objective of this work to continue the subject further.

3.8 Summary

We have considered an 1D model for the close-packed lines of potassium ions inside a cation layer of mica muscovite using realistic potentials. There exists only a single kink with a specific velocity and energy dubbed the crowdion. It is relatively well described by the magic mode but the kink is transformed into a double kink. A construction in terms of phasors has been developed in order to obtain an intuition of the relative phases and behaviour of the particles as the kink passes over them. The crowdion leaves behind a phonon wave with exponentially diminishing amplitude that travels at the same velocity as that of the kink. Simulations with different initial energies bring about a variety of phenomena including the formation of two crowdions that leave behind nonlinear waves and phonons. The crowdions also survive at temperatures of 300–1000 K. Finally, an analysis of the possible decay modes of ^{40}K has been performed including their possible consequences with respect to the

formation of crowdions and other lattice excitations. A careful study of the tracks in mica muscovite compared with the decay modes could shed light on the track characteristics and origin.

The energy of the kinks or crowdions described in this chapter can be provided by the ^{40}K decay and is enough to expel an atom at the border. The crowdions survive to high temperature and travel long distances. They transport positive charge and therefore are very likely to be recorded in the form of dark tracks in mica muscovite. If they are the cause of the quodons or other marks observed in this mineral is still an open question.

Acknowledgments J.F.R.A., V.S.M., and L.M.G.R. acknowledge financial support from the projects FIS2008-04848, FIS2011-29731-C02-02, and MTM2012-36740-C02-02 from Ministerio de Ciencia e Innovación (MICINN). All authors acknowledge Prof. F.M. Russell for ongoing discussions.

References

1. Archilla, J.F.R., Kosevich, Yu.A., Jiménez, N., Sánchez-Morcillo, V.J., García-Raffi, L.M.: Moving excitations in cation lattices. Ukr. J. Phys. **58**(7), 646–656 (2013)
2. Archilla, J.F.R., Kosevich, Yu.A., Jiménez, N., Sánchez-Morcillo, V.J., García-Raffi, L.M.: Supersonic kinks in Coulomb lattices. In: Carretero-González, R. et al. (eds.) Localized Excitations in Nonlinear Complex Systems, pp. 317–331. Springer, New York (2014)
3. Archilla, J.F.R., Kosevich, Yu.A., Jiménez, N., Sánchez-Morcillo, V.J., García-Raffi, L.M.: Ultradiscrete kinks with supersonic speed in a layered crystal with realistic potentials. Phys. Rev. E **91**, 022912 (2015)
4. Cameron, J.A., Singh, B.: Nuclear data sheets for A=40. Nucl. Data Sheets **102**(2), 293–513 (2004)
5. Collins, D.R., Catlow, C.R.A.: Computer simulation of structure and cohesive properties of micas. Am. Mineral. **77**(11–12), 1172–1181 (1992)
6. Diaz, M., Farmer, V.C., Prost, R.: Characterization and assignment of far infrared absorption bands of K^+ in muscovite. Clays Clay Miner. **48**, 433–438 (2000)
7. Durrani, S.A.: Nuclear tracks today: strengths, weaknesses, challenges. Rad. Meas **43**, S26–S33 (2008)
8. Engelkemeir, D.W., Flynn, K.F., Glendenin, L.E.: Positron emission in the decay of K^{40}. Phys. Rev. **126**(5), 1818–1822 (1962)
9. Fleischer, R.: Nuclear tracks in science and technology. Tracks to Innovation. Springer, New York (2011)
10. Friesecke, G., Matthies, K.: Atomic-scale localization of high-energy solitary waves on lattices. Physica D **171**(4), 211–220 (2002)
11. Gedeon, O., Machacek, J., Liska, M.: Static energy hypersurface mapping of potassium cations in potassium silicate glasses. Phys. Chem. Glass. **43**(5), 241–246 (2002)
12. Korteweg, D.J., de Vries, F.: On the change of form of long waves advancing in a rectangular canal, and on a new type of long stationary waves. Philos. Mag. **39**, 422–443 (1895). http://en.wikipedia.org/wiki/Korteweg-de_Vries_equation
13. Kosevich, A.M., Kovalev, A.S.: The supersonic motion of a crowdion. The one dimensional model with nonlinear interaction between the nearest neighbors. Solid State Commun. **12**, 763–764 (1973)
14. Kosevich, Yu.A.: Nonlinear sinusoidal waves and their superposition in anharmonic lattices. Phys. Rev. Lett. **71**, 2058–2061 (1993)

15. Kosevich, Yu.A., Khomeriki, R., Ruffo, S.: Supersonic discrete kink-solitons and sinusoidal patterns with magic wave number in anharmonic lattices. Europhys. Lett. **66**, 21–27 (2004)
16. Kudriavtsev, Y., Villegas, A., Godines, A., Asomoza, R.: Calculation of the surface binding energy for ion sputtered particles. Appl. Surf. Sci. **239**(3–4), 273–278 (2005)
17. Lide, D.R. (ed.): Handbook of Chemistry and Physics, 90th edn., Sect. 10, p. 203. CRC Press, Boca Raton (2010)
18. Milchev, A.: Breakup threshold of solitons in systems with nonconvex interactions. Phys. Rev. B **42**, 6727–6729 (1990)
19. Molerón, M., Leonard, A., Daraio, C.: Solitary waves in a chain of repelling magnets. J. Appl. Phys. **115**(18), 184901 (2014)
20. Mougeot, X., Helmer, R.G.: LNE-LNHB/CEA-Table de Radionucléides, K-40 tables. http://www.nucleide.org (2012)
21. Pradler, J., Singh, B., Yavin, I.: On an unverified nuclear decay and its role in the DAMA experiment. Phys. Lett. B **720**(4–5), 399–404 (2013)
22. Price, P.B., Walker, R.M.: Observation of fossil particle tracks in natural micas. Nature **196**, 732–734 (1962)
23. Russell, F.M.: The observation in mica of tracks of charged particles from neutrino interactions. Phys. Lett. **25B**, 298–300 (1967)
24. Russell, F.M.: Tracks in mica caused by electron showers. Nature **216**, 907–909 (1967)
25. Russell, F.M.: Identification and selection criteria for charged lepton tracks in mica. Nucl. Tracks. Rad. Meas. **15**, 41–44 (1988)
26. Russell, F.M.: I saw a crystal. In: Archilla, J.F.R., Jiménez, N., Sánchez-Morcillo, V.J., García-Raffi, L.M. (eds.) Quodons in Mica: Nonlinear Localized Travelling Excitations in Crystals, pp. 475–559. Springer (2015)
27. Russell, F.M.: Tracks in mica, 50 years later. In: Archilla, J.F.R., Jiménez, N., Sánchez-Morcillo, V.J., García-Raffi, L.M. (eds.) Quodons in Mica: Nonlinear Localized Travelling Excitations in Crystals, pp. 3–33. Springer (2015)
28. Russell, F.M., Collins, D.R.: Lattice-solitons and non-linear phenomena in track formation. Rad. Meas **25**, 67–70 (1995)
29. Russell, F.M., Collins, D.R.: Lattice-solitons in radiation damage. Nucl. Instrum. Meth. B **105**, 30–34 (1995)
30. Russell, F.M., Eilbeck, J.C.: Evidence for moving breathers in a layered crystal insulator at 300 K. Europhys. Lett. **78**, 10004 (2007)
31. Russell, F.M., Eilbeck, J.C.: Persistent mobile lattice excitations in a crystalline insulator. Discret. Contin. Dyn. S.-S **4**, 1267–1285 (2011)
32. Savin, A.V.: Supersonic regimes of motion of a topological soliton. Sov. Phys. JETP **81**(3), 608–613 (1995)
33. Schlößer, D., Kroneberger, K., Schosnig, M., Russell, F.M., Groeneveld, K.O.: Search for solitons in solids. Rad. Meas **23**, 209–213 (1994)
34. Sinev, V.V., Bezrukov, L.B., Litvinovich, E.A., Machulin, I.N., Skorokhvatov, M.D., Sukhotin, S.V.: Looking for antineutrino flux from 40K with large liquid scintillator detector. Phys. Part. Nuclei **46**(2), 186–189 (2015)
35. Steeds, J.W., Russell, F.M., Vine, W.J.: Formation of epidote fossil positron tracks in mica. Optik **92**, 149–154 (1993)
36. Ziegler, J.F., Biersack, J.P., Ziegler, M.D.: SRIM—The Stopping and Range of Ions in Matter. James Ziegler, Chester (2008)
37. Zolotaryuk, Y., Eilbeck, J.C., Savin, A.V.: Bound states of lattice solitons and their bifurcations. Physica D **108**, 81–91 (1997)